Polarization Effects in Intermediate Temperature, Anode-Supported Solid Oxide Fuel Cells

Journal of The Electrochemical Society, **146** (1) 69-78 (1999)
S0013-4651(98)05-091-5 CCC: $7.00 © The Electrochemical Society, Inc.

Polarization Effects in Intermediate Temperature, Anode-Supported Solid Oxide Fuel Cells

Jai-Woh Kim,[a,*] Anil V. Virkar,[a,*] Kuan-Zong Fung,[a,*] Karun Mehta,[*,a] and Subhash C. Singhal[b,*]

[a]*Department of Materials Science and Engineering, University of Utah, Salt Lake City, Utah 84112, USA*
[b]*Westinghouse Electric Corporation, Pittsburgh, Pennsylvania 15235, USA*

Anode-supported solid oxide fuel cells with yttria-stabilized zirconia (YSZ) electrolyte, Sr-doped $LaMnO_3$ (LSM)+ YSZ cathode, and Ni + YSZ anode were fabricated and their performance was evaluated between 650 and 800°C with humidified hydrogen as the fuel and air as the oxidant. Maximum power densities measured were ~1.8 W/cm^2 at 800°C and ~0.82 W/cm^2 at 650°C. Voltage (V) vs. current density (i) traces were nonlinear; V vs. i exhibited a concave-up curvature [$d^2V/di^2 \geq 0$] at low values of i and a convex-up curvature [$d^2V/di^2 \leq 0$] at higher values of i, typical of many low temperature fuel cells. Analysis of concentration polarization based on transport of gaseous species through porous electrodes, in part, is used to explain nonlinear V vs. i traces. The effects of activation polarization in the Tafel limit are also included. It is shown that in anode-supported cells, the initial concave-up curvature can be due either to activation or concentration polarization, or both. By contrast, in cathode-supported cells, the initial concave-up curvature is entirely due to activation polarization. From the experimentally observed V vs. i traces for anode-supported cells, effective binary diffusivity of gaseous species on the anodic side was estimated to be between ~0.1 cm^2/s at 650°C and ~0.2 cm^2/s at 800°C. The area specific resistance of the cell (ohmic part), varied between ~0.18 Ω cm^2 at 650°C and ~0.07 Ω cm^2 at 800°C with an activation energy of ~65 kJ/mol.

Manuscript received May 28, 1998.

Solid oxide fuel cells (SOFCs) have received considerable attention for use in the direct conversion of chemical energy of a fuel into electrical energy. Currently, there are three basic designs of SOFCs under development. These are electrolyte-supported, cathode-supported, and anode-supported. In electrolyte-supported cells, the thickness of the electrolyte, typically yttria-stabilized zirconia (YSZ), is ≥150 μm with thin electrodes screen printed on it.[1,2] In such cells the ohmic contribution is large (due to high electrolyte resistivity) and such cells are being envisioned for operation at ~1000°C where the electrolyte resistivity is low, typically ~20 Ω cm. In cathode-supported cells, such as those in the Westinghouse tubular design, a layer of YSZ 30 to 40 μm in thickness is deposited on a porous Sr-doped $LaMnO_3$ (LSM) cathode of a thickness ~2 mm. [3] Similarly, in anode-supported cells, a YSZ layer of 10 to 20 μm thickness is deposited on a relatively thick Ni + YSZ anode.[4,5] In electrode-supported designs, the ohmic contribution is smaller than in the electrolyte-supported cells. In addition, the contribution of activation polarization is also expected to be lower, especially with the use of composite electrodes in which the reaction zone spreads out into the electrodes.[6-10] Thus, electrode-supported design in principle is better suited for operation at lower temperatures. However, in electrode-supported cells, a significant contribution may well arise from concentration polarization resulting from the resistance to gas transport through thick, porous electrodes.[11,12] It is thus imperative that the electrode structure be optimized to minimize both activation and concentration polarizations.

A number of research groups are currently pursuing anode-supported cells. Using relatively thin anodes, cells exhibiting a high performance at a temperature as low as 800°C have been demonstrated. For example, in a recent paper, de Souza et. al.[13] reported a power density as high as about 1.9 W/cm^2 at 800°C using anode-supported (~200 μm thick anode) cells. The V vs. i traces in their study were nonlinear with a concave-up curvature [$d^2V/di^2 \geq 0$] at low current densities and a convex-up curvature [$d^2V/di^2 \leq 0$] at higher current densities. This type of a behavior is typically observed in low temperature fuel cells (phosphoric acid, for example).[14] The initial concave-up curvature [$d^2V/di^2 \geq 0$] is generally attributed to activation polarization while the convex-up curvature [$d^2V/di^2 \leq 0$] at higher current densities is attributed to concentration polarization.[14] In SOFCs operating at high temperatures (~1000°C), activation polarization can exhibit an essentially ohmic behavior over a wide range in current densities and thus may be represented in terms of a charge-transfer resistance. Indeed, measurements of Yamamoto et al.[c,15] show that a plot between overpotential and current density is nearly linear up to $i \approx 1$ A/cm^2. Also, exchange current density, i_o, in excess of 200 mA/cm^2 has been reported at high temperatures (≥800°C).[16] If such high exchange current densities are indeed possible, the nonlinearity in V vs. i traces at low i in electrode-supported SOFCs then cannot be automatically attributed to activation polarization. In fact, in the case of cathode-supported SOFCs investigated at Westinghouse, when tested at 1000°C, the initial concave-up region is not observed, and the V vs. i trace is convex-up over the entire range of current densities.[17] If the relation between current density and overpotential could be described by the Tafel limit, which would be the case for small i_o, the curvature in V vs. i traces in cathode-supported cells will also be expected to be concave-up at low current densities. For example, Ippommatsu et al. observed that in their cathode-supported cells, the V vs. i traces were concave-up at low current densities.[18] As is discussed later, in the case of ohmic activation polarization (large i_o), V vs. i traces for anode-supported and cathode-supported cells in general are expected to be different.

The principal objective of the present work was to fabricate anode-supported cells, test them over a range of temperatures, and evaluate their performance. Cells with a sufficiently large anode thickness (≥700 μm) were fabricated so that they are quite rugged and can be easily handled. Performance of the cells was measured between 650 and 800°C. Relatively large anode thickness requires the incorporation of concentration polarization into the analysis of V vs. i traces. A simple analysis of concentration polarization based on binary diffusion through porous electrodes, along with activation polarization in the Tafel limit was used to analyze the V vs. i traces and estimate polarization losses.

Experimental

Cell fabrication.—NiO and 8 mol % YSZ powders obtained from commercial sources were weighed in desired proportions, typically 50 vol % of each, and mixed in ethanol for 24 h. After the removal of volatiles, disks ~32 mm in diam were die-pressed in a uniaxial press followed by isostatic pressing at pressures up to 200 MPa. A slurry of YSZ in ethanol was prepared and disks were coated with the slurry. The disks were then sintered in air at 1400°C for 1 h. LSM powder of

** Electrochemical Society Active Member.
* Electrochemical Society Fellow.

[c] Yamamoto et al.[15] plotted η vs. ln i and observed a nonlinear dependence. However, their data when plotted on a linear scale, i.e., η vs. i, is a straight line up to current densities as high as ~1 A/cm^2.

S0013-4651(98)05-091-5 CCC: $7.00

stoichiometry $La_{0.8}Sr_{0.2}MnO_{(3-\delta)}$ was prepared by calcining a mixture of La_2O_3, $SrCO_3$, and MnO_2 in air at 1000°C. The calcined LSM powder was subsequently ballmilled. A mixture containing LSM and YSZ powders in equal amounts (by weight) was made and mixed with an organic liquid to form a paste. The paste was applied over the sintered disks (on the dense YSZ layer). The disks were then heated to 400°C to burn out volatiles. This procedure was repeated until a layer of 50 to 70 μm thickness was formed. The disks were later heated to 1250°C for 1 h. This thermal treatment was adequate to ensure the formation of a good bond between the porous LSM + YSZ cathode and the underlying dense YSZ layer, but without forming a significant amount of highly resistive $La_2Zr_2O_7$ pyrochlore phase. Cells were fractured after testing and examined under a scanning electron microscope.

Cell testing.—The single cell test stand consists of two alumina tubes in between which a cell can be secured. Silver wire meshes were used as current collectors which were pressed against the cathode and the anode with a thin layer of platinum resinate in between to ensure a good bond between the silver meshes and the electrodes. The cell was secured between two inconel bushings with mica gaskets. Silver current leads were affixed to the two silver meshes. The cell was placed inside the furnace. The test stand was designed in such a way that the seals (gaskets) were always under a spring loading with springs outside the furnace. Thus, no glass seal was necessary. This permitted repeated heating/cooling of the cells and retesting. Hydrogen as a fuel was bubbled through water maintained at ~33°C and circulated past the anode, and ambient air was circulated past the cathode. Temperature was varied between 650 and 800°C. Reduction of NiO into Ni was accomplished in situ. Cell performance was measured using an electronic load. Figure 1 shows a schematic diagram of the testing apparatus.

Results

Several cells were tested to determine performance over a range of temperatures between 650 and 800°C. Table I gives the maximum power densities at four temperatures on three cells from the same batch. After the tests, the cells were fractured and examined under a scanning electron microscope. Figure 2 is a scanning electron micrograph of a fractured anode-supported cell showing part of the porous cathode, the dense electrolyte, and part of the porous anode. As evident in the figure, the YSZ layer is essentially fully dense with no open porosity. The cathode, the electrolyte, and the anode thicknesses were, respectively, about 50, 10, and 750 μm. The anode porosity was measured to be ~38 vol %. The cathode porosity was not measured on this cell but was estimated to be about ~30 vol % based on measurements made on thicker LSM + YSZ porous composites made separately. Figure 3a shows the results on one of the cells in which the voltage (V) is plotted vs. current density (i) at four temperatures: 650, 700, 750, and 800°C. The short-circuit current density at 800°C was about of 5.6 A/cm^2 and that at 650°C was about 3.15 A/cm^2. The V vs. i traces exhibit a concave-up curvature [$d^2V/di^2 \geq 0$] at low current densities, followed by an approximately linear behavior, and followed by a convex-up curvature [$d^2V/di^2 \leq 0$] at higher current densities. Slopes of linear regions of the voltage vs. current density plots were estimated at the four temperatures. This slope is effectively the area specific cell resistance, R_{cell}, usually referred to as the ohmic contribution.[19] The R_{cell} should contain at a minimum the area specific resistance of the electrolyte, $\rho_e \ell_e$, where ρ_e is the electrolyte resistivity and ℓ_e is the electrolyte thickness, and the effective charge-transfer or polarization resistance, R_{ct}^{eff}, which is a measure of the activation polarization, if it can be assumed to be ohmic. In addition, it should also contain some contribution from concentration polarization as is discussed later. Slope of V vs. i traces as $i \rightarrow 0$ was also determined. The inset in Fig. 3a shows a plot of ln (R_{cell}/T) vs. $1/T$, where T is the temperature in kelvin, from the slope of which, an activation energy, Q_{cell} of ~50 kJ/mol. is measured. Figure 3b shows the corresponding power density as a function of i. The maximum power densities measured were ~0.82 W/cm^2 at 650°C and ~1.8 W/cm^2 at 800°C.

Table I. Maximum power density.

T (°C)	Cell 1 (W/cm^2)	Cell 2 (W/cm^2)	Cell 3 (W/cm^2)
650	0.77	0.83	0.86
700	1.08	1.18	1.08
750	1.31	1.47	1.39
800	1.58	1.80	1.64

Theoretical Analysis

Transport through porous electrodes.—The fundamental equations governing the isothermal transport of gaseous species through porous electrodes for a mixture of two gases, A and B, are given by[20]

$$J_A = -D_A \nabla n_A + X_A \delta_A J - X_A \gamma_A \left(\frac{nB_o}{\mu} \right) \nabla p \qquad [1a]$$

$$J_B = -D_B \nabla n_B + X_B \delta_B J - X_B \gamma_B \left(\frac{nB_o}{\mu} \right) \nabla p \qquad [1b]$$

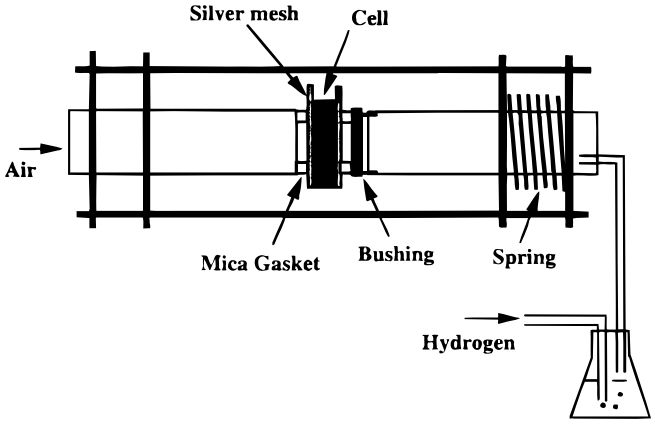

Figure 1. A schematic diagram of a single cell test setup.

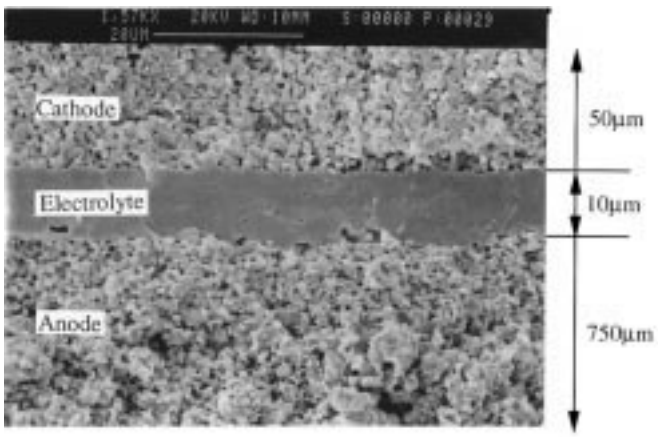

Figure 2. A scanning electron micrograph (SEM) of a fractured cell showing part of the porous cathode, the dense electrolyte, and part of the porous anode.

S0013-4651(98)05-091-5 CCC: $7.00

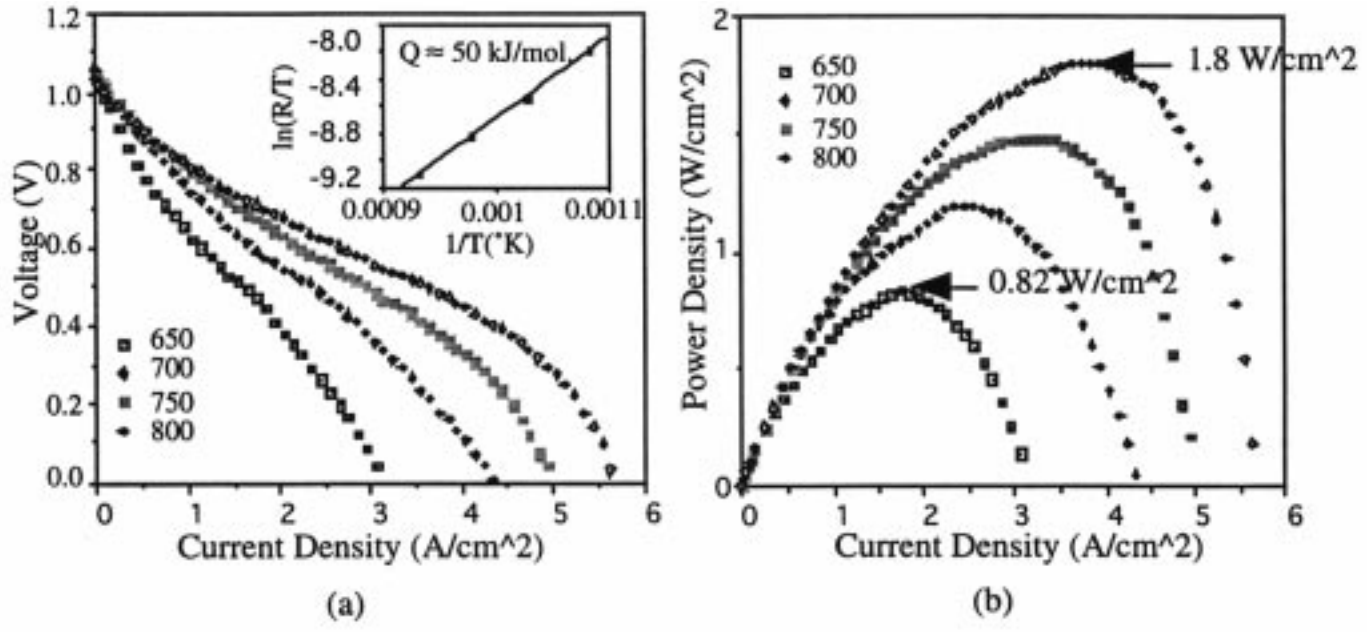

Figure 3. (a) Voltage (V) vs. current density (i) for an anode-supported single cell at four temperatures; 650, 700, 750, and 800°C. (b) Power density vs. current density (i).

where

$$\frac{1}{D_A} = \frac{1}{D_{AK}} + \frac{1}{D_{AB(eff)}} \qquad \delta_A = \frac{D_{AK}}{D_{AK} + D_{AB(eff)}}$$

$$\frac{1}{D_B} = \frac{1}{D_{BK}} + \frac{1}{D_{AB(eff)}} \qquad \delta_B = \frac{D_{BK}}{D_{BK} + D_{AB(eff)}}$$

$$\gamma_A = \frac{D_{AB}}{D_{AK} + D_{AB(eff)}} \qquad \gamma_B = \frac{D_{AB}}{D_{BK} + D_{AB(eff)}} \qquad [2]$$

In the above equations, J_A and J_B are fluxes of A and B, respectively, $D_{AB(eff)}$ is the effective binary diffusivity (modified to account for porosity and tortuosity), D_{AK} and D_{BK} are Knudsen diffusivities, n_A and n_B are the concentrations (no./cm^3), $n = (n_A + n_B)$, X_A and X_B are the mole fractions, B_o is the permeability, μ is the viscosity, p is the total pressure, and J is the total flux. Parameters δ_A and δ_B and γ_A and γ_B are as defined above. Equations 1a and 1b include two flux contributions; a diffusive flux and a viscous flow. The diffusive contribution consists of two terms; free molecule or Knudsen flow (defined by terms containing D_{AK} and D_{BK}), and a continuum part. Typical total pressure on the anodic and cathodic sides is on the order of 1 atm or greater, and the typical pore size is ≥ 1 μm. Thus, in general, D_{AK} and $D_{BK} >> D_{AB(eff)}$, and D_A and D_B can be replaced by $D_{AB(eff)}$.[d,20] That is, at high pressures, such as those of interest here, both D_A and D_B approach $D_{AB(eff)}$, the effective binary diffusion coefficient, δ_A and $\delta_B \to 1$, and γ_A and $\gamma_B \to 0$. Thus, the main contribution to the total flux is due to continuum diffusion. The effective binary diffusivity, $D_{AB(eff)}$, is given by binary diffusivity, D_{AB}, multiplied by the volume fraction of porosity, V_v, and divided by the tortuosity factor, τ.[20,21] Usually, the tortuosity factor, τ, varies between two and ten for many porous bodies, especially those with a relatively coarse pore structure.[21] For the cathode, the D_{AB} refers to the binary diffusion coefficient for a mixture of oxygen, O_2, and nitrogen, N_2. On the anode side, the requisite binary diffusion coefficient is that for H_2 and H_2O. Experimental measurements of binary diffusion coefficients for various gas pairs are available at 1 atm pressure at selected temperatures; at room temperature, $D_{O_2-N_2} \approx 0.22$ cm^2/s and $D_{H_2-H_2O} \approx 0.91$ cm^2/s.[21] The dependence of diffusion coefficient on temperature is not very strong and to a first approximation it may be modified using the kinetic theory of gases. This suggests that concentration polarization effects in general should be less on the anode side. The following analysis is based on the assumption that the dominant contribution to gas transport through the porous electrodes is by binary diffusion.

Figure 4 shows schematic diagrams of anode-supported and cathode-supported solid oxide fuel cells. If the porosity and the microstructure of the electrode are functions of position, and/or D_{AB} is composition-dependent, the variation of partial pressures of the various species with position will not be linear. For this reason, the schematics given in Fig. 4 show nonlinear variation of partial pressures.

In a steady state, the following equality must hold

$$\left|j_{H_2}\right| = \left|j_{H_2O}\right| = 2\left|j_{O_2}\right| = \frac{iN_A}{2F} \qquad [3]$$

If the electrode microstructure is not a function of position, and D_{AB} is composition-independent, the simplest description of transport is given by diffusion wherein the binary diffusion coefficient is modified by porosity and tortuosity of the electrodes. In the case of anode with the only gases being H_2 and H_2O (partial pressure of oxygen being much lower), for a fixed total pressure, Eq. 1a and 1b reduce to

$$J_{H_2} = -\frac{D_a V_{v(a)}}{\tau_a} \nabla n_{H_2} \qquad [4]$$

$$J_{H_2O} = -\frac{D_a V_{v(a)}}{\tau_a} \nabla n_{H_2O} \qquad [5]$$

since $J_{H_2} + J_{H_2O} = 0$. In terms of the current density, i, partial pressures of hydrogen, $p_{H_2(a)}$, and water vapor, $p_{H_2O(a)}$, at the anode/electrolyte interface, are given by

$$p_{H_2(a)} = p^o_{H_2} - \frac{RT}{2FD_a} \frac{\tau_a l_a}{V_{v(a)}} i \qquad [6]$$

$$p_{H_2O(a)} = p^o_{H_2O} + \frac{RT}{2FD_a} \frac{\tau_a l_a}{V_{v(a)}} i \qquad [7]$$

[d] However, if the pore size is very small and the tortuosity factor is large, Knudsen diffusion may have to be taken into account.

S0013-4651(98)05-091-5 CCC: $7.00

On the cathode side, the flux of nitrogen is zero. Thus, Eq. 1a and 1b for a fixed total pressure, p, reduce to

$$J_{O_2} = -\frac{D_c V_{v(c)}}{\tau_c} \nabla n_{O_2} + X_{O_2} J_{O_2} \quad [8]$$

For a cathode thickness of l_c with spatially invariant porosity and tortuosity, the partial pressure of oxygen at the cathode/electrolyte interface is given by

$$p_{O_2(c)} = p - (p - p^o_{O_2}) \exp\left[\frac{iRT\tau_c l_c}{4FD_c p V_{v(c)}}\right] \quad [9]$$

For an anode-supported cell with a small cathode thickness, the exponent can be shown to be typically much less than one. Thus, expanding the exponential term and retaining only the first two terms give

$$p_{O_2(c)} \approx p^o_{O_2} - \left(\frac{p - p^o_{O_2}}{p}\right)\frac{RT\tau_c l_c}{4FD_c V_{v(c)}} i \quad [10]$$

In what follows, the above, simplified equation is used which leads to simple analytical solutions.

The partial pressure of oxygen, $p_{O_2(a)}$, at the anode/electrolyte interface is given in terms of $p_{H_2(a)}$ and $p_{H_2O(a)}$ and the equilibrium constant, K_{eq}, for the reaction

$$H_2(g) + \frac{1}{2}O_2(g) \rightarrow H_2O(g)$$

by

$$p_{O_2(a)} = \frac{1}{K^2_{eq}}\left(\frac{p^o_{H_2O} + \frac{RT}{2FD_a}\frac{\tau_a l_a}{V_{v(a)}} i}{p^o_{H_2} - \frac{RT}{2FD_a}\frac{\tau_a l_a}{V_{v(a)}} i}\right)^2 \quad [11]$$

Parameters f and g are defined in what follows as

$$f = \frac{RT}{4FD_c}\frac{\tau_c l_c}{V_{v(c)}} \quad [12]$$

$$g = \frac{RT}{2FD_a}\frac{\tau_a l_a}{V_{v(a)}} \quad [13]$$

If both the porosity and the tortuosity are functions of position, but D_{AB} is composition-independent, then the effective electrode microstructural multipliers are given by

$$\left(\frac{\tau_c l_c}{V_{v(c)}}\right)_{eff} = \int_0^{l_c}\frac{\tau_c(x)dx}{V_{v(c)}(x)} \quad [14]$$

$$\left(\frac{\tau_a l_a}{V_{v(a)}}\right)_{eff} = \int_0^{l_a}\frac{\tau_a(x)dx}{V_{v(a)}(x)} \quad [15]$$

The corresponding partial pressures at the electrolyte/electrode interfaces are given by

$$p_{H_2(a)} = p^o_{H_2} - \frac{RT}{2FD_a}\left(\frac{\tau_a l_a}{V_{v(a)}}\right)_{eff} i \quad [16]$$

$$p_{H_2O(a)} = p^o_{H_2O} + \frac{RT}{2FD_a}\left(\frac{\tau_a l_a}{V_{v(a)}}\right)_{eff} i \quad [17]$$

$$p_{O_2(c)} \approx p^o_{O_2} - \left(\frac{p - p^o_{O_2}}{p}\right)\frac{RT}{4FD_c}\left(\frac{\tau_c l_c}{V_{v(c)}}\right)_{eff} i \quad [18]$$

The corresponding parameters f and g are then given by

$$f = \frac{RT}{4FD_c}\left(\frac{\tau_c l_c}{V_{v(c)}}\right)_{eff} \quad [19]$$

$$g = \frac{RT}{2FD_a}\left(\frac{\tau_a l_a}{V_{v(a)}}\right)_{eff} \quad [20]$$

The effective binary diffusion coefficients for the anode and the cathode gases can be defined as

$$D_{a(eff)} = \frac{D_a V_{v(a)}}{\tau_a} = \frac{D_a l_a}{\left(\frac{\tau_a l_a}{V_{v(a)}}\right)_{eff}} \quad [21]$$

$$D_{c(eff)} = \frac{D_c V_{v(c)}}{\tau_c} = \frac{D_c l_c}{\left(\frac{\tau_c l_c}{V_{v(c)}}\right)_{eff}} \quad [22]$$

For electrode microstructure invariant with position, the partial pressures of hydrogen, and water vapor in the anode, and of oxygen[e] in the cathode are expected to vary linearly with position in the electrodes for most of the electrode thickness. However, near the electrode/electrolyte interfaces, variation of the partial pressures is expected to be nonlinear (and also rapid) despite a spatially invariant microstructure. This is because the process of charge transfer occurs

[e] Only for a thin cathode.

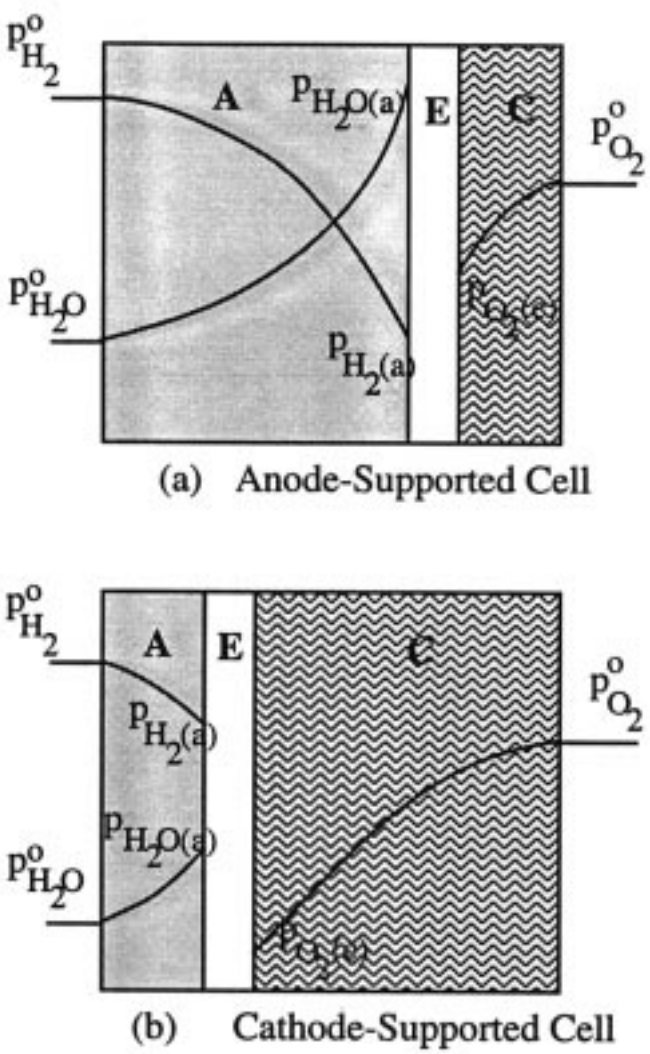

Figure 4. Schematic diagrams of anode-supported and cathode-supported solid oxide fuel cells.

S0013-4651(98)05-091-5 CCC: $7.00

over a certain thickness of the composite electrode from the electrode/electrolyte interface.[6-10] Over this region, the net current consists of both ionic and electronic contributions, both functions of position. Outside this region, the current is purely electronic in the electrodes and purely ionic in the electrolyte.

Effective charge-transfer resistance of composite electrodes.—The process of charge transfer in porous composite electrodes has been examined by many investigators, dating back to the original work by Newman and Tobias.[6] The composite electrode problem as applied to solid-state electrochemical devices has been examined by Kenjo et al.,[7,8] Deng et al.,[9] and by Tanner et al.[10] The results of these analyses show that the reaction zone is spread out into the electrode some distance from the electrolyte/electrode interface. Tanner et al.[10] defined an effective charge-transfer resistance, R_{ct}^{eff}, in terms of microstructural parameters of the electrode, intrinsic charge-transfer resistance,[f] R_{ct}, ionic conductivity of the electrolyte part of the composite electrode, σ_e, and the electrode thickness, h. The effective charge-transfer resistance, R_{ct}^{eff}, is given by Ref. 10

$$R_{ct}^{eff} = \frac{BR_{ct}}{B\left(\frac{1+\beta}{1+\beta\,\exp\left(-\frac{2h}{\alpha}\right)}\right)(1-V_v)\,\exp\left(-\frac{h}{\alpha}\right) + \left(\frac{1+\beta\,\exp\left(-\frac{h}{\alpha}\right)}{1+\beta\,\exp\left(-\frac{2h}{\alpha}\right)}\right)\alpha\left(1-\exp\left(-\frac{h}{\alpha}\right)\right) + BV_v} \quad [23]$$

where

$$\alpha = \sqrt{\sigma_e B(1-V_v)R_{ct}} \quad \text{and} \quad \beta = \frac{\sigma_e R_{ct} - \alpha}{\sigma_e R_{ct} + \alpha} \quad [24]$$

in which V_v denotes fractional porosity. Equation 23 shows that the effective charge-transfer resistance, R_{ct}^{eff}, approaches R_{ct} as $h \to 0$, and decreases with increasing electrode thickness. It can be shown that as $h \to \infty$, the R_{ct}^{eff} is given by Ref. 10

$$R_{ct}^{eff} \approx \sqrt{\frac{BR_{ct}}{\sigma_e(1-V_v)}} \quad [25]$$

Equations 23 and 25 also show the effect of microstructural dimension, B, which is essentially the grain size of the electrolyte material (YSZ here) in the electrode. Analysis by Kenjo et al.[7] as well as by Tanner et al.[10] predicts a limiting value of the R_{ct}^{eff} as $h \to \infty$, here given by Eq. 25. It is seen that R_{ct}^{eff} depends upon R_{ct}, σ_e, and B. The functional form of Eq. 25 is such that a limiting value is reached when $h \geq l_{ct}$ where l_{ct}, which is a measure of the extent to which the reaction zone spreads from the electrolyte/electrode interface into the electrode, depends on a microstructural parameter such as B. It can be shown that for $B \approx 1$ μm, the estimated value of l_{ct} is about 10 μm. [10] That is, the reaction zone spreads about 10 μm from the electrolyte/electrode interface into the electrode, which is a small fraction of the total thickness of either of the electrodes. Therefore, in the analysis presented here, it is assumed that the effective electrolyte area specific resistance, R_i, is given by the sum of the electrolyte area specific resistance, R_{el}, and the effective charge-transfer resistance given by Eq. 25, R_{ct}^{eff}; that is, $R_i = R_{el} + R_{ct}^{eff} = \rho_e \ell_e + R_{ct}^{eff} = \ell_e/\sigma_e + R_{ct}^{eff}$. Thus, the partial pressures of gaseous species at the electrolyte/electrode interfaces, $p_{H_2(a)}$, $p_{H_2O(a)}$, $p_{O_2(a)}$, and $p_{O_2(c)}$, are effectively the partial pressures just outside the reaction zones.

Although the preceding assumes activation polarization as being ohmic, it is not necessary to so assume. In fact, as discussed later, at least on the cathode side, the Tafel equation may adequately describe the process of charge transfer. In such a case also, the reaction zone spreads out some distance from electrolyte/electrode interface into the electrode.

Voltage (V) vs. current density (i) traces.—Equating the fluxes as given in Eq. 3, and substituting for the various interface partial pressures in terms of the current density, i, the relationship between the voltage across load, $V(i)$, and i is given by

$$V(i) = E_{(s)}^o - iR_i + \frac{RT}{4F}\ln\left(p_{O_2}^o - \left(\frac{p - p_{O_2}^o}{p}\right)fi\right) + \frac{RT}{2F}\ln(p_{H_2}^o - gi) - \frac{RT}{2F}\ln(p_{H_2O}^o + gi) \quad [26]$$

This equation is similar to the one given by McDougall[14] with the exception of the term containing $\ln(p_{H_2O}^o + gi)$, the significance of which is discussed shortly.

When $i = 0$, that is corresponding to the open-circuit limit

$$V(0) = E_{(s)}^o + \frac{RT}{4F}\ln\left(\frac{p_{O_2}^o\,p_{H_2}^{o\,2}}{p_{H_2O}^{o\,2}}\right) = E_o \quad [27]$$

where E_o is the open-circuit voltage (OCV). When $V = 0$, the corresponding short-circuit current density, i_s, is given by

$$i_s = \frac{E_{(s)}^o}{R_i} + \frac{RT}{4FR_i}\ln\left\{\frac{p_{O_2}^o - \left(\frac{p - p_{O_2}^o}{p}\right)fi_s}{\left(\frac{p_{H_2O}^o + gi_s}{p_{H_2}^o - gi_s}\right)}\right\} \quad [28]$$

Current density-dependent area specific resistance of the cell is the negative gradient of the $V(i)$ and i trace, namely

$$R(i) = -\frac{dV(i)}{di} = R_i + \frac{RT}{4F}\left\{\frac{\left(\frac{p - p_{O_2}^o}{p}\right)f}{p_{O_2}^o - \left(\frac{p - p_{O_2}^o}{p}\right)fi} + \frac{2g}{p_{H_2}^o - gi} + \frac{2g}{p_{H_2O}^o + gi}\right\} \quad [29]$$

or

$$R(i) = R_i + \frac{RT}{4F}\left\{\frac{\left(\frac{p - p_{O_2}^o}{p}\right)f}{p_{O_2(c)}} + \frac{2g}{p_{H_2(a)}} + \frac{2g}{p_{H_2O(a)}}\right\} \quad [30]$$

The current density-independent term, R_i, is the area specific resistance of the cell inclusive of the effective charge-transfer resistance, R_{ct}^{eff}, a measure of the activation polarization, assumed here to be ohmic. The remaining term, which is current density-dependent, is

[f] Intrinsic charge-transfer resistance, R_{ct}, is defined here as the charge-transfer resistance measured when the electrocatalyst is deposited on a planar electrolyte surface. This R_{ct} is essentially equal to RT/zFi_o. Thus, R_{ct} is not only a function of the particular electrocatalyst but also its particle size and amount since this effectively defines the three-phase boundary (TPB) length per unit area of the electrocatalyst/electroyte (planar) interface.

S0013-4651(98)05-091-5 CCC: $7.00

the contribution of concentration polarization to the cell resistance, $R_{conc}(i)$, given by

$$R_{conc}(i) = \frac{RT}{4F}\left\{\frac{\left(\frac{p - p^o_{O_2}}{p}\right)f}{p^o_{O_2} - \left(\frac{p - p^o_{O_2}}{p}\right)fi} + \frac{2g}{p^o_{H_2} - gi} + \frac{2g}{p^o_{H_2O} + gi}\right\}$$

$$= \frac{RT}{4F}\left\{\frac{\left(\frac{p - p^o_{O_2}}{p}\right)f}{p_{O_2(c)}} + \frac{2g}{p_{H_2(a)}} + \frac{2g}{p_{H_2O(a)}}\right\} \quad [31]$$

When $i = 0$, the $R_{conc}(i)$ reduces to

$$R_{conc}(0) = \frac{RT}{4F}\left\{\frac{\left(\frac{p - p^o_{O_2}}{p}\right)f}{p^o_{O_2}} + \frac{2g}{p^o_{H_2}} + \frac{2g}{p^o_{H_2O}}\right\} \quad [32]$$

which is nonzero indicating that the effect of concentration polarization persists even at the open-circuit limit. Effectively, the greater the magnitude of the slope of $V(i)$ vs. i as $i \to 0$, the greater is the $R_{conc}(0)$. Also, as is evident from Eq. 32, the lower the $p^o_{H_2O}$, i.e., the drier the incoming fuel, the greater is the $R_{conc}(0)$, and effectively the greater is the initial concavity in the $V(i)$ and i trace. Equation 28 is the general expression for the short-circuit current density, i_s. Corresponding to this current density, the sum of ohmic, activation, and concentration overpotentials equals the open-circuit potential. Neither the partial pressure of hydrogen at the electrolyte/anode interface, $p_{H2(a)}$, nor the partial pressure of oxygen at the electrolyte/cathode interface, $p_{O2(c)}$, need be near zero. However, if one of the electrodes is considerably thicker than the other, the i_s can be a limiting current density dictated by the electrode thickness wherein the requisite partial pressure at the interface is near zero.[14] In anode-supported cells with $l_a >> l_c$, the limiting current density, i_{as}, when $p_{H2(a)} \approx 0$, is given by

$$i_{as} = \frac{p^o_{H_2}}{g} = \frac{2D_aF}{RT}\frac{p^o_{H_2}}{\left[\frac{\tau_a l_a}{V_{v(a)}}\right]} = \frac{2D_aF}{RT}\frac{p^o_{H_2}}{\int_0^{l_a}\frac{\tau_a(x)\,dx}{V_{v(a)}(x)}}$$

$$= \frac{2Fp^o_{H_2}D_{a(eff)}}{RTl_a} \quad [33]$$

In cathode-supported cells with $l_c >> l_a$, the limiting current density, i_{cs}, when $p_{O2(c)} \approx 0$, is given by setting Eq. 9 to zero. Here we define i_{cs} by setting Eq. 10 to zero which is for small values of l_c. Thus, it is to be noted that the value of i_{cs} here is not the i_{cs} that would be applicable to thick cathodes. The i_{cs} is defined here by

$$i_{cs} = \frac{p^o_{O_2}}{\left(\frac{p - p^o_{O_2}}{p}\right)f} = \frac{4D_cF}{RT\left[\frac{\tau_c l_c}{V_{v(c)}}\right]}\frac{p^o_{O_2}}{\left(\frac{p - p^o_{O_2}}{p}\right)}$$

$$= \frac{4D_cF}{RT\int_0^{l_c}\frac{\tau_c(x)\,dx}{V_{v(c)}(x)}}\frac{p^o_{O_2}}{\left(\frac{p - p^o_{O_2}}{p}\right)} = \frac{4Fp^o_{O_2}D_{c(eff)}}{\left(\frac{p - p^o_{O_2}}{p}\right)RTl_c} \quad [34]$$

In terms of the limiting current densities, i_{as} and i_{cs}, the $V(i)$ vs. i relation can be given by

$$V(i) = E^o_{(s)} + \frac{RT}{4F}\ln\left(\frac{p^o_{O_2}p^{o^2}_{H_2}}{p^{o^2}_{H_2O}}\right) - iR_i + \frac{RT}{4F}\ln\left(1 - \frac{i}{i_{cs}}\right)$$

$$+ \frac{RT}{2F}\ln\left(1 - \frac{i}{i_{as}}\right) - \frac{RT}{2F}\ln\left(1 + \frac{p^o_{H_2}i}{p^o_{H_2O}i_{as}}\right) \quad [35]$$

or

$$V(i) = E_o - iR_i + \frac{RT}{4F}\ln\left(1 - \frac{i}{i_{cs}}\right) + \frac{RT}{2F}\ln\left(1 - \frac{i}{i_{as}}\right)$$

$$- \frac{RT}{2F}\ln\left(1 + \frac{p^o_{H_2}i}{p^o_{H_2O}i_{as}}\right) \quad [36]$$

This equation is similar to the one given by McDougall[14] with the exception of the last term. If the i_s is limited by electrode thickness, the corresponding slope of the $V(i)$ vs. i trace as $i \to i_{as}$ will approach $-\infty$; that is, the $V(i)$ vs. i trace will be nearly vertical as $i \to i_s$. The $R(i)$ can be given in terms of the limiting current densities as follows

$$R(i) = R_i + \frac{RT}{4F}\left\{\frac{1}{(i_{cs} - i)} + \frac{2}{(i_{as} - i)} + \frac{2}{\left(\frac{p^o_{H_2O}}{p^o_{H_2}}i_{as} + i\right)}\right\} \quad [37]$$

As is evident from Eq. 37, $R(i) \to \infty$ as $i \to i_{as}$ or as $i \to i_{cs}$. Although the equation also shows that $R(i) \to \infty$ as $i \to i_{cs}$, it is to be noted that a simplification was previously made that the exponent in Eq. 9 is much less than one. Thus, the above equation is applicable only under such conditions. That is, the equation given above is applicable to anode-supported cells where $i_{as} \leq i_{cs}$. Figure 3a shows that the $V(i)$ vs. i traces at 650 and 700°C do not meet the current density axis vertically at the i_s indicating that a limiting current density had not reached under the experimental conditions. By contrast, at 750 and 800°C, the $V(i)$ vs. i traces appear to meet the i axis nearly vertically. It would thus appear that i_s at 750 and 800°C is close to the limiting current density, i_{as}.

In terms of i_{as} and i_{cs}, the concentration polarization resistance at OCV is given by

$$R_{conc}(0) = \frac{RT}{4F}\left\{\frac{1}{i_{cs}} + \frac{2}{i_{as}}\left(1 + \frac{p^o_{H_2}}{p^o_{H_2O}}\right)\right\} \quad [38]$$

Note that the drier the incoming fuel, the larger is the $R_{conc}(0)$.

Shape of the voltage (V) vs. current density (i) traces.—The second derivative of $V(i)$ vs. i is given by

$$\frac{d^2V(i)}{di^2} = -\frac{RT}{4F}\left\{\frac{\left[\left(\frac{p - p^o_{O_2}}{p}\right)f\right]^2}{\left(p^o_{O_2} - \left(\frac{p - p^o_{O_2}}{p}\right)fi\right)^2} + \frac{2g^2}{\left(p^o_{H_2} - gi\right)^2}\right.$$

$$\left. - \frac{2g^2}{\left(p^o_{H_2O} + gi\right)^2}\right\} \quad [39]$$

S0013-4651(98)05-091-5 CCC: $7.00

or

$$\frac{d^2V(i)}{di^2} = -\frac{RT}{4F}\left\{\frac{1}{(i_{cs}-i)^2} + \frac{2}{(i_{as}-i)^2} - \frac{2}{\left(\frac{p^o_{H_2O}}{p^o_{H_2}} i_{as} + i\right)^2}\right\} \quad [40]$$

which describes the curvature. Equations 39 and 40 show that in general anode-supported and cathode-supported cells are expected to exhibit different behaviors. For cathode-supported cells, $((p - p^o_{O_2})/p)f >> g$ ($i_{cs} << i_{as}$), and the second and third terms in the parenthesis containing g (or i_{as}) may be ignored (provided $p^o_{H_2O}$ is not too small) in relation to the first term containing f (or i_{cs}). Thus

$$\frac{d^2V(i)}{di^2} \approx -\frac{RT}{4F}\frac{\left[\left(\frac{p - p^o_{O_2}}{p}\right)f\right]^2}{\left(p^o_{O_2} - \left(\frac{p - p^o_{O_2}}{p}\right)fi\right)^2} = -\frac{RT}{4F}\left(\frac{1}{(i_{cs}-i)^2}\right) \quad [41]$$

which is always less than zero; that is $d^2V/di^2 \leq 0$. Thus, over the entire current density regime, the curvature of $V(i)$ vs. i should be convex-up. Work done at Westinghouse on cathode-supported cells tested at 1000°C shows this indeed is the case.[17] By contrast, for anode-supported cells with $g >> ((p - p^o_{O_2})/p)f$ ($i_{as} << i_{cs}$), and the first term in parenthesis containing f (or i_{cs}) can be ignored in relation to the second and third terms containing g (or i_{as}). Thus

$$\frac{d^2V(i)}{di^2} \approx -\frac{RTg^2}{2F}\left\{\frac{1}{\left(p^o_{H_2} - gi\right)^2} - \frac{1}{\left(p^o_{H_2O} + gi\right)^2}\right\}$$

$$= -\frac{RT}{2F}\left\{\frac{1}{(i_{as}-i)^2} - \frac{1}{\left(\frac{p^o_{H_2O}}{p^o_{H_2}} i_{as} + i\right)^2}\right\} \quad [42]$$

As i increases, the first term in Eq. 42 increases in magnitude while the second term decreases. Note that in general $p^o_{H_2} >> p^o_{H_2O}$. Thus, at small current densities, $1/(p^o_{H_2O} + gi)^2 > 1/(p^o_{H_2} - gi)^2$ or $1/(p^o_{H_2O}/p^o_{H_2} i_{as} + i)^2 > 1/(i_{as} - i)^2$ and $d^2V(i)/di^2 > 0$. That is, the $V(i)$ vs. i trace at small values of i will be concave-up. At higher current densities, however, it is possible that $1/(p^o_{H_2} - gi)^2 > 1/(p^o_{H_2O} + gi)^2$ or $1/(i_{as} - i)^2 > 1/(p^o_{H_2O}/p^o_{H_2} i_{as} + i)^2$ and correspondingly $d^2V(i)/di^2 < 0$. That is, the $V(i)$ vs. i trace at large i will exhibit a convex-up curvature. Whether or not a convex-up curvature is observed at high values of i will depend upon the magnitude of R_i. If R_i is large, the current density corresponding to $d^2V(i)/di^2 = 0$ may be greater than i_s. In such a case, a convex-up region may not be observed. Experimental results given in Figure 3a show that in the present case, $d^2V(i)/di^2 < 0$ at high current densities. For anode-supported cells with $g >> ((p - p^o_{O_2})/p)f$, from the inflexion point, i.e., $d^2V(i)/di^2 = 0$, one can obtain the parameter g, which is given by $g = (p^o_{H_2} - p^o_{H_2O})/2i^*$ where i^* is the current density at the inflexion point. Alternatively, if g is large (due either to a very thick anode and/or low porosity and/or high tortuosity), the i^* may be very low. In such case, inflexion will occur at very low current densities and the $V(i)$ vs. i trace will be convex-up for most of the current density regime.

Inclusion of nonohmic activation polarization.—The discussion so far assumes activation polarization as being ohmic. As the anode structure is very fine and prior work has shown cathode polarization is usually larger than anode polarization, the assumption of ohmic activation polarization for the anode may be reasonable. However, this may not be the case with the cathode. For large current densities, the Tafel equation is often applicable. In what follows, activation polraization in the Tafel limit is included.

When the electrode kinetics are very sluggish, the exchange current density, i_o, is low and over the range of interest of i, the Tafel equation adequately describes the relation between i and η_{act}, given by

$$\eta_{act} = a + b \ln i \quad [43]$$

where the a and b are of the form

$$a \approx -\frac{RT}{4\alpha F} \ln i_o \quad \text{and} \quad b \approx \frac{RT}{4\alpha F} \quad [44]$$

where i_o is the exchange current density and α is the transfer coefficient. In what follows, a and b are treated simply as empirical constants. Inclusion of activation polarization into the equation for $V(i)$ vs. i gives

$$V(i) = E_o - iR_i - a - b \ln i + \frac{RT}{4F} \ln\left(1 - \frac{i}{i_{cs}}\right) + \frac{RT}{2F} \ln\left(1 - \frac{i}{i_{as}}\right) - \frac{RT}{2F} \ln\left(1 + \frac{p^o_{H_2} i}{p^o_{H_2O} i_{as}}\right) \quad [45]$$

and the corresponding current density dependent cell resistance is given by

$$R(i) = -\frac{dV(i)}{di} = R_i + \frac{b}{i} + \frac{RT}{4F}\left\{\frac{1}{(i_{cs}-i)} + \frac{2}{(i_{as}-i)} + \frac{2}{\left(\frac{p^o_{H_2O}}{p^o_{H_2}} i_{as} + i\right)}\right\} \quad [46]$$

The experimental data can be fitted to Eq. 45 with five parameters, namely, R_i, i_{as}, i_{cs}, a, and b.

Comparison of Experimental Results with Analysis and Discussion

V(i) vs. traces.—All $V(i)$ vs. i traces shown in Fig. 3a exhibit the expected behavior for anode-supported cells (with low R_i); ($d^2V/di^2 \geq 0$) at low current densities, and ($d^2V/di^2 \leq 0$) at higher current densities. The experimental $V(i)$ vs. i trace at each temperature was fitted using five adjustable parameters: R_i, i_{as}, i_{cs}, a, and b. These parameters were adjusted to obtain the best possible fit to Eq. 45. Figure 5 compares the best fit to experimental data at 800°C. The fit is not very sensitive to the value of i_{cs} as long as $i_{cs} > i_{as}$, consistent with expectations for an anode-supported cell. Thus, the value of i_{cs} is not particularly accurate (nor important as long as $i_{cs} > i_{as}$). Table II gives the parameters R_i, i_{as}, a, and b corresponding to the best fits at the four temperatures tested. The R_i, which primarily consists of the electrolyte area specific resistance, R_{el}, and any ohmic part of the activation polarization (R^{eff}_{ct}), e.g., from the anode side, varies between 0.178 Ω cm^2 (1.78×10^{-5} Ω m^2) at 650°C and 0.068 Ω cm^2 (6.8×10^{-6} Ω m^2) at 800°C. The electrolyte thickness was about 10 μm. For a measured resistivity of 50 Ω cm at 800°C, the calculated value of the electrolyte area specific resistance is about 0.05 Ω cm^2. The R_i from the curve fit should consist of the electrolyte resistance, R_{el}, and possible ohmic part of the activation polarization (possibly from the anode). Thus, the agreement between the fitted parameter and that estimated from experimentally measured resistivity on a pellet is quite good. As

S0013-4651(98)05-091-5 CCC: $7.00

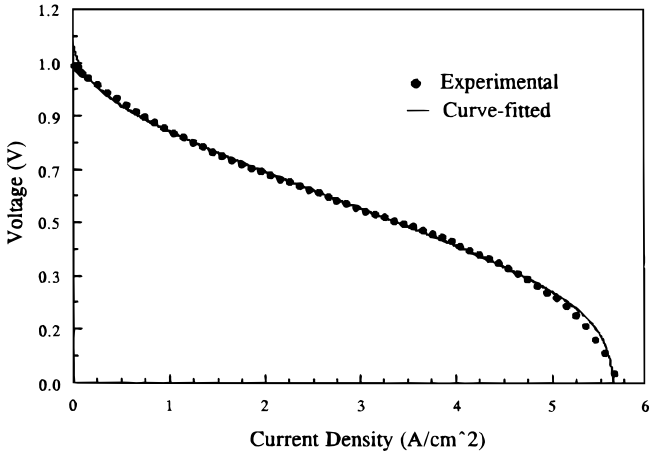

Figure 5. Experimental data at 800°C and the corresponding best fit to Eq. 45.

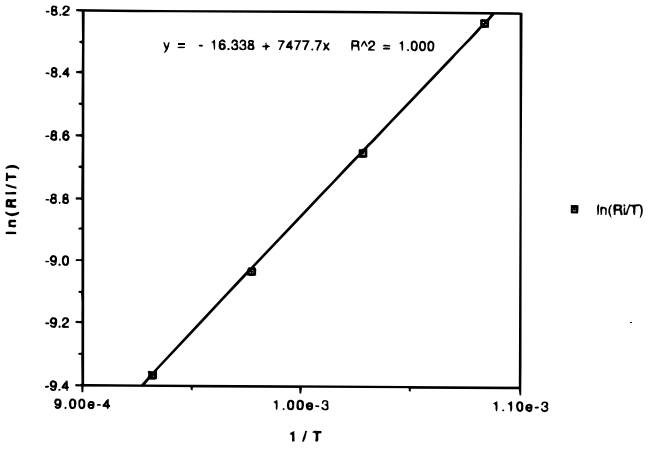

Figure 6. A plot ln (R_i/T) vs. 1/T. The activation energy, Q_i, is ~65 kJ/mol.

shown in Fig. 6, ln (R_i/T) vs. 1/T is nearly linear with an activation energy (Q_i) of ~65 kJ/mol. The temperature range of measurements (150 K) is too small in the present experiments to yield an accurate estimate of the activation energy. Thus activation energies reported here should only be regarded as crude estimates. The activation energy for ionic conduction in YSZ, Q_e, is reported to be ~95 kJ/mol.[22] Our measurement of Q_e on a dense YSZ pellet is about 87 kJ/mol.

The exchange current density, i_o, estimated from the fitted a and b is given in Table II. It varies between ~51 mA/cm^2 at 650°C to ~132 mA/cm^2 at 800°C. A high i_o has been achieved through the use of composite electrodes.[10] It can be readily demonstrated that without the use of composite electrodes, the estimated i_o is typically less than 10 mA/cm^2 at 800°C. The parameter b is defined in Eq. 44). For each of the four temperatures, comparison of the estimated parameter b with Eq. 44 gives an estimate of the transfer coefficient, α. The value of α was found to between ~0.64 at 650°C and ~0.93 at 800°C. No specific interpretation can be given to α obtained here, except to note that it is not unreasonable.[23]

As the cathode thickness is much smaller than the anode thickness, $i_{cs} >> i_{as}$, and the curve fit is not very sensitive to the value of i_{cs} (as long as $i_{cs} > i_{as}$). Thus, no estimate of the i_{cs} or $D_{c(eff)}$ can be made from the present work. However, from the fitted anode limiting current density, i_{as}, the effective diffusion coefficients on the anode side, $D_{a(eff)}$ can be obtained. The estimated $D_{a(eff)}$ (Table II) varies between ~0.096 cm^2/s (~9.6×10^{-6} m^2/s) at 650°C and ~0.199 cm^2/s (~1.99×10^{-5} m^2/s) at 800°C. The observed increase in $D_{a(eff)}$ with an increase in temperature is consistent with expectations. Theoretical expression for a binary diffusion coefficient in the gas phase is given by Chapman-Enskogg model[21] as follows

$$D_{12} \approx \frac{0.00186T^{\frac{3}{2}}\left(\frac{1}{M_1}+\frac{1}{M_2}\right)^{\frac{1}{2}}}{p\sigma_{12}^2\Omega} \qquad [47]$$

where M_1 and M_2 are molecular weights of the two species, Ω is the collision integral, and σ_{12} is the collision diameter. Equation 47 shows that the $D_{12} \propto T^{1.5}$. In the present work, diffusion occurs through a porous electrode and the interaction of gas molecules with the porous medium may be considerably more complex than assumed.[20] Further, the neglect of Knudsen diffusion may also not be entirely justified. Thus, an exact agreement is not to be expected. Nevertheless, the estimated $D_{a(eff)}$ plotted vs. $T^{1.5}$ in Fig. 7 shows that the plot is indeed linear. However, the intercept when extrapolated to $T = 0$ is not zero as required by Eq. 47. The intercept is negative indicating that the dependence of $D_{a(eff)}$ on T is stronger than predicted by the Chapman-Enskogg model. Thus, the agreement between the estimated $D_{a(eff)}$ and expectations of Chapman-Enskogg model is considered to be only fair. The model nevertheless may be used to obtain an approximate value of the tortuosity factor. Using Eq. 47 and values of relevant parameters given in Ref. 21, $D_{H_2-H_2O}$ at 800°C was estimated to be 7.6×10^{-4} m^2/s. The estimated $D_{a(eff)}$

Table II. Measured and fitted parameters for the anode-supported cell.

Temperature (°C)	650	700	750	800
R_i (Ω cm^2)	0.178	0.139	0.092	0.068
a	0.0923	0.0628	0.054	0.050
b	0.031	0.0281	0.0248	0.0247
$\frac{RT}{4F}$	0.01988	0.02096	0.02204	0.0232
i_o (A/cm^2)	0.051	0.107	0.113	0.132
i_{as} (A/cm^2)	3.18	4.74	4.95	5.65
i_s (A/cm^2) (measured)	3.15	4.4	5.0	5.6
$D_{eff(a)} = \frac{RTl_a}{2Fp^o_{H_2}} i_{as}$ (cm^2/s)	0.096	0.151	0.166	0.199
R_{cell} (Ω cm^2)	0.255	0.189	0.151	0.130
From the linear region of $V(i)$ vs. i				
$R_{cell}(0) - R_i$ (Ω cm^2)	0.391	0.289	0.24	0.193
$R_{conc}(0) \approx \frac{RT}{2Fi_{as}}\left(1+\frac{p^o_{H_2}}{p^o_{H_2O}}\right)$ (Ω cm^2)	0.417	0.31	0.297	0.273
$R_{cell(0)}$ (Ω cm^2) (measured)	0.569	0.428	0.332	0.261

S0013-4651(98)05-091-5 CCC: $7.00

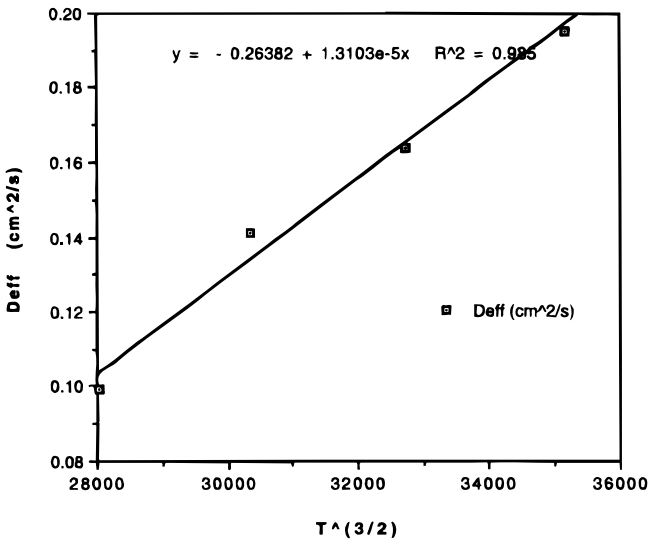

Figure 7. A plot of the estimated $D_{a(eff)}$ vs. $T^{1.5}$ from the anode-supported cell.

at 800°C from curve fitting to the $V(i)$ vs. i trace is 1.99×10^{-5} m^2/s. From this, the combined porosity-tortuosity factor is estimated as the ratio of $D_{H_2-H_2O}$ and $D_{a(eff)}$ which is ~38.2. The porosity is 38% or $V_{v(a)} \approx 0.38$. Thus, the tortuosity factor on the anode side, τ_a, is estimated to be ~14.5. The tortuosity factor is typically between two and six with values as high as ten also been reported.[21] The majority of the reported measurements are on porous bodies with a relatively coarse structure. In the present work, typical pore size is on the order of a few microns. Thus, the estimated value of ~14.5 is quite reasonable.

Table II also lists the measured cell resistance at zero current, i.e., $R_{cell}(0)$, as the magnitude of the slope of $V(i)$ vs. i trace as $i \rightarrow 0$. This slope contains the electrolyte resistance, R_i, concentration polarization, $R_{conc}(0)$, and a contribution from the activation term. The table lists $R_{cell}(0)$ obtained by extrapolating from current densities $i > i_o$. It may then be assumed that the main contributions are from R_i and $R_{conc}(0)$. The table also lists the difference $R_{cell}(0) - R_{conc}(0)$. From the curve fitted parameters, the values of i_{as} are known. Thus, $R_{conc}(0)$ can be obtained from Eq. 38 (ignoring the term with i_{cs}). This value is also given in Table II. As seen in the table, the estimated values of $R_{conc}(0)$ are in reasonable agreement with experimentally measured $R_{cell}(0) - R_{conc}(0)$ at all temperatures except at 800°C. It is to be mentioned that a great deal of uncertainty exists in the determination of $R_{conc}(0)$ by extrapolating $V(i)$ vs. i trace as $i \rightarrow 0$ insofar as the range over which extrapolation is made.

Conclusions

In the present work, anode-supported solid oxide fuel cells with Ni + YSZ as the anode, YSZ as the electrolyte, and LSM + YSZ as the cathode were fabricated and tested over a range of temperatures between 650 and 800°C. Maximum power densities measured were ~0.82 W/cm^2 at 650°C and ~1.8 W/cm^2 at 800°C. The $V(i)$ vs. i traces exhibited a concave-up curvature at low current densities and a convex-up curvature at higher current densities. This behavior can be adequately described in terms of both concentration and activation polarizations. A simple analysis describing fuel cell performance based on the assumption of binary diffusion as the dominant mode of gas transport through porous electrodes was presented. From the analysis of $V(i)$ vs. i traces, effective binary diffusivity on the anode side, $D_{a(eff)}$, was estimated. High values of exchange current densities (>100 mA/ cm^2 at 800°C) demonstrate the effectiveness of the composite cathode in substantially reducing the polarization resistance.

Acknowledgments

This work was supported by the Electric Power Research Institute, Gas Research Institute, and the State of Utah under its Centers of Excellence Program.

The University of Utah assisted in meeting the publication costs of this article.

List of Symbols

B_o	permeability
D_{AB}	binary diffusivity of A and B, cm^2/s or m^2/s
D_{AK}	Knudsen diffusivity, cm^2/s or m^2/s
D_a	binary diffusion coefficient on the anode side (between H_2 and H_2O), cm^2/s or m^2/s
D_c	binary diffusion coefficient on the cathode side (between O_2 and N_2), cm^2/s or m^2/s
$D_{eff(a)}$	effective diffusion coefficient on the anode side (between H_2 and H_2O), cm^2/s or m^2/s
$D_{eff(c)}$	effective diffusion coefficient on the cathode side (between O_2 and N_2), cm^2/s or m^2/s
$E^o_{(s)}$	standard Nernst potential, V
E_o	open-circuit voltage, V
F	Faraday constant, C/mol
i	current density, A/cm^2 or A/m^2
i_s	short-circuit current density, A/cm^2 or A/m^2
i_{cs}	limiting current density (cathode-limited), A/cm^2 or A/m^2
i_{as}	limiting current density (anode-limited), A/cm^2 or A/m^2
j_{H_2}	flux of hydrogen through porous anode
j_{H_2O}	flux of water vapor through porous anode
j_{O_2}	flux of oxygen through porous cathode
k_B	Boltzmann constant, erg/K
l_a	anode thickness, cm or m
l_c	cathode thickness, cm or m
l_{ct}	region over which charge transfer occurs. In general, this is expected to be different for the anode and the cathode, cm or m
ℓ_e	electrolyte thickness, cm or m
M_1	molecular weight of gas 1
M_2	molecular weight of gas 2
N	Avogadro's number
n_A and n_B	concentrations of A and B, respectively
p	pressure, Pa
$p^o_{H_2}$	partial pressure of hydrogen in the fuel (outside of the anode), Pa or atm
$p^o_{H_2O}$	partial pressure of water vapor in the fuel (outside of the anode), Pa or atm
$p^o_{O_2}$	partial pressure of oxygen in the oxidant (outside of the cathode), Pa or atm
$p_{H_2(a)}$	partial pressure of hydrogen at the anode/electrolyte interface, Pa or atm
$p_{H_2O(a)}$	partial pressure of water vapor at the anode/electrolyte interface, Pa or atm
$p_{O_2(a)}$	partial pressure of oxygen at the anode/electrolyte interface, Pa or atm
$p_{O_2(c)}$	Partial pressure of oxygen at the cathode/electrolyte interface, Pa or atm
R	gas constant, J/mol deg
R_{el}	electrolyte area specific resistance (without the charge-transfer resistance), Ω cm^2 or Ω m^2.
R_i	area specific resistance of the electrolyte (including charge-transfer resistance), Ω cm^2 or Ω m^2. In general, $R_i = R_{el} + R^{eff}_{ct}$.
R_{cell}	area specific (current density dependent) cell resistance, Ω cm^2 or Ω m^2
R_{conc}	area specific (current density dependent) concentration polarization resistance, Ω cm^2 or Ω m^2
R_{ct}	intrinsic (area specific) charge-transfer resistance, Ω cm^2 or Ω m^2
R^{eff}_{ct}	effective (area specific) charge-transfer resistance, Ω cm^2 or Ω m^2
$R(i)$	current density-dependent area specific resistance of the cell, Ω cm^2 or Ω m^2
T	temperature, °C or K
$V(i)$	voltage across load, V
$V_{v(a)}$	anode porosity
$V_{V(c)}$	cathode porosity
Greek	
μ	viscosity
σ_e	ionic conductivity of the electrolyte, S/cm or S/m = $1/\rho_e$
σ_{12}	effective collision diameter, cm or m
τ_a	anode tortuosity factor
τ_c	cathode tortuosity factor

References

1. N. Hisatome and K. Nagata, S. Kakigami, and H. Omura, in Fuel Cell Seminar Program and Abstracts, 1996 Fuel Cell Seminar, p. 194, Orlando, FL, Nov 17-20, 1996.

S0013-4651(98)05-091-5 CCC: $7.00

2. Y. Miyake, M. Kadowaki, Y. Akiyama, T. Yasuo, S. Taniguchi, K. Nishio, in Fuel Cell Seminar Program and Abstracts, p. 28, 1996 Fuel Cell Seminar, Orlando, FL, Nov 17-20, 1996.
3. S. C. Singhal, Abstract 2136, p. 2498, The Electrochemical Society Meeting Abstracts, Vol. 92-2, Paris, France, Aug 31-Sept 5, 1997.
4. N. Q. Minh, *J. Am. Ceram. Soc.*, **76**, 563 (1993).
5. H. P. Buchkremer, U. Diekmann, L. G. J. de Haart, H. Kabs, U. Stimming, and D. Stover, in *Proceedings of 1996 Fuel Cell Seminar*, sponsored by the Fuel Cell Organizing Committee, pp. 175-178, Washington, DC (1996).
6. J. S. Newman and C. Tobias, *J. Electrochem. Soc.*, **109**, 1183 (1962).
7. T. Kenjo, S. Osawa, and K. Fujikawa, *J. Elctrochem. Soc.*, **138**, 349 (1991).
8. T. Kenjo and M. Nishiya, *Solid State Ionics*, **57**, 295 (1992).
9. H. Deng, M. Zhou, and B. Abeles, *Solid State Ionics*, **74**, 75 (1994).
10. C. W. Tanner, K-Z. Fung, and A. V. Virkar, *J. Electrochem. Soc.*, **144**, 21-30 (1997).
11. K. Z. Fung and A. V. Virkar, in *Proceedings of the 4th International Symposium on Solid Oxide Fuel Cells (SOFC-IV)*, M. Dokiya, O. Yamamoto, H. Tagawa, and S. C. Singhal, Editors, PV 95-1, p. 1105, The Electrochemical Society Proceedings Series, Pennington, NJ (1995).
12. T. Kenjo and Y. Yamakoshi, *Bull. Chem. Soc. Jpn.*, **65**, 995 (1992).
13. S. de Souza, S. J. Visco, and L. C. De Jonghe, *J. Electrochem. Soc.*, **144**, L35 (1997).
14. A. McDougall, *Fuel Cells*, MacMillan Press, London (1976).
15. O. Yamamoto, Y. Takeda, N. Imanashi, and Y. Sakaki, in *Proceedings of the 3rd International Symposium on Solid Oxide Fuel Cells*, S. C. Singhal and H. Iwahara, Editors, PV 93-4, p. 205, The Electrochemical Society Proceedings Series, Pennington, NJ (1993).
16. K. Wipperman, U. Stimming, H. Jansen, and D. Stöver, in *Proceedings of the 3rd International Symposium on Solid Oxide Fuel Cells*, S. C. Singhal and H. Iwahara, Editors, PV 93-4, p. 180, The Electrochemical Society Proceedings Series, Pennington, NJ (1993).
17. S. C. Singhal, in *Proceedings of the 5th International Symposium on Solid Oxide Fuel Cells (SOFC-V)*, U. Stimming, S. C. Singhal, H. Tagawa, and W. Lennert, PV 97-40, p. 37, The Society Proceedings Series, Pennington, NJ (1995).
18. A. Kajimura, H. Sasaki, S. Otoshi, M. Suzuki, C. Kurusu, N. Sugiura, and M. Ippommatsu, in *Proceedings of the 3rd International Symposium on Solid Oxide Fuel Cells*, S. C. Singhal and H. Iwahara, Editors, PV 93-4, p. 395, The Electrochemical Socity Proceedings Series, Pennington, NJ (1993).
19. J. H. Hirschenhofer, D. B. Stauffer, and R. R. Engleman, *Fuel Cells: A Handbook*, (Revision 3), U.S. Department of Energy, Office of Fossil Energy, METC, Morgantown, WV (1994).
20. E. A. Mason and A. P. Malinauskas, *Gas Transport in Porous Media: The Dusty Gas Model*, Elsevier, Amsterdam (1983).
21. E. L. Cussler, *Diffusion: Mass Transfer in Fluid Systems*, Cambridge University Press, Cambridge (1995).
22. T. H. Etsell and S. N. Flengas, *Chem. Rev.*, **70**, 339 (1970).
23. D. R. Crow, *Principles and Applications of Electrochemistry*, Blackie Academic & Professional, London (1994).